J Mater Sci: Mater Electron (2023)34:392

The effect of thermal evaporation parameters on thermoelectric properties of $Bi_2Te_{2.7}Se_{0.3}$ thin films produced from ball milled powder

Yasaman Saberi[1] and Seyed Abdolkarim Sajjadi[1,*]

[1] *Department of Materials Science and Engineering, Ferdowsi University of Mashhad, Mashhad 9177948974, Iran*

Received: 16 November 2022
Accepted: 28 December 2022

ABSTRACT

This research aims to expand the knowledge related to the thermoelectric efficiency of $Bi_2Te_{2.7}Se_{0.3}$ thin films in order to enhance the property. Therefore, in the present study, $Bi_2Te_{2.7}Se_{0.3}$ thin films were fabricated by mechanical alloying and thermal evaporation procedures. The effects of deposition parameters including the substrate temperature and the annealing temperature on the x-ray diffraction pattern, microstructure, and optical and thermoelectric properties were evaluated. The results showed that the substrate temperature and the annealing temperature are effective on microstructure, crystallinity, chemical composition and thermoelectric properties of thin films. All of the samples showed the p-type conductor due to the presence of antisites in the samples (Bi_{Te} as acceptors and hole producers). Among the samples, the thin film deposited at the substrate temperature of 50 °C and annealed at 50 °C (BS50A50) showed the significant increment in the power factor (0.88 $\mu W/K^2$ cm) Moreover, the thin film showed the favorable Seebeck coefficient (59 $\mu V/K$) and electrical conductivity (257 S/cm). The results were due to the homogeneity, crystallinity and tiny pores of the sample BS50A50.

1 Introduction

The global warming problems and the energy saving requirements have attracted a lot of attention from researchers to work on sustainable energy [1–3]. In this regard, thermoelectric materials have been investigated by researchers because of their desired and attractive properties. It should be noted that thermoelectric materials have been considered for the conversion of heat energy to electricity or vice versa [4, 5]. Furthermore, the increasing demand for using thin film electronic devices from the aspect of miniaturization instruments has stimulated scientists to work on thin film thermoelectric materials [6, 7].

Thin film materials have been used in different applications e.g., sensors, chip-spots, refrigerators and wearable electronic devices [8–10]. Based on the literature [11, 12], $Bi_2Te_{2.7}Se_{0.3}$ thin film materials show the best thermoelectric properties compared with Bi_2Te_3 materials. It can be related to the strong

Address correspondence to E-mail: sajjadi@um.ac.ir

https://doi.org/10.1007/s10854-022-09804-3
Published online: 04 February 2023

electromigration of Se atoms compared with Te atoms and the effect of this parameter on the lattice strain, dislocation density, appropriate crystallite size and grain size in $Bi_2Te_{2.7}Se_{0.3}$ thin film materials. As indicated in the literature, $Bi_2Te_{2.7}Se_{0.3}$ compound compared with Bi_2Te_3, shows higher thermoelectric performance due to the less porosity and favorable grain size caused by the presence of Se content [13, 14]. In addition, the optimum amount of grain size is essential to the enhancement of the Seebeck coefficient, the electrical conductivity and thus, the power factor. The property relates to Se content and the production method. According to the literature, the ternary alloy of $Bi_2Te_{2.7}Se_{0.3}$ is known as semiconductor material with high thermoelectric performance [11, 12, 15].

In recent years, different methods such as ball milling [16–19] and hydrothermal [14] as well as gas atomization [20, 21] have been used to produce Bi_2Te_3 based alloys. Moreover, several procedures e.g., thermal evaporation [22], sputtering [23], laser deposition [24] and flash evaporation [25, 26] have been applied for the manufacturing of Bi_2Te_3 based thin film materials. According to previous studies, long operational life, different sizes and no emission of toxic gasses are the advantages of thermoelectric thin films [14, 17]. However, the low conversion efficiency is the main challenge of thermoelectric materials. Therefore, the attempts have been made to enhance the power factor of thin films. It should be mentioned that power factor is calculated based on the equation of $PF = S^2\delta$. In this equation, S is the Seebeck coefficient and δ is the electrical conductivity [16, 17]. This parameter is required to evaluate the thermoelectric performance of materials.

One of the parameters affecting thermoelectric properties of thin film materials is the temperature of annealing followed by the deposition process [22, 25, 27]. Brougault et al. [28] reported the effect of the annealing process on the thermoelectric properties of $Bi_2Te_{2.7}Se_{0.3}$ thin film produced by sputtering technique. According to the report, the annealing temperature plays the main role in the variations of crystallization, defects and atomic composition of thin films. Duan et al. [25] manufactured $Bi_2Te_{2.7}Se_{0.3}$ thin films deposited by flash evaporation procedure. Based on the research, the temperature of the annealing process (373–573 K) influenced the thermoelectric properties. The results showed that the annealing temperature of 473 K leads to the maximum power factor (12 $\mu W/K^2{\cdot}cm$). The effect of annealing temperature can be observed on carrier concentration and mobility of carriers. The optimum amount of carrier concentration and antistructure defects can be obtained by suitable annealing temperature. Lin et al. [29] produced Bi_2Te_3 thin films by thermal evaporation method. The study proved that the increase in the annealing temperature leads to the reduction of the carrier concentration and increase of the Seebeck coefficient. The electrical conductivity reached the maximum amount with optimizing the annealing temperature and time. Therefore, the adjustment of temperature and time of the annealing process is important. Obviously, $Bi_2Te_{2.7}Se_{0.3}$ thin films have a wide range of applications from cooling systems to sensors. Hence, evaluation of the procedures for improvement of the power factor in these novel materials is required.

In addition to the annealing parameters, the substrate temperature is the other key factor affecting the improvement of the power factor and in turn, the thermoelectric performance of thin films [24, 30]. Wudil et al. [24] investigated $Bi_2Te_{2.7}Se_{0.3}$ thin film materials deposited by pulse laser deposition. In that study, the substrate temperature was changed between 200 and 400 °C and the maximum power factor was achieved at 300 °C. A decline in the Seebeck coefficient after 300 °C was related to the lower crystallinity and a slight Te deficiency which led to an increase in the carrier concentration.

Lin et al. [30] investigated the effect of substrate temperature (from room temperature up to 150 °C) on thermoelectric properties of Sb_2Te_3 thin films deposited by thermal evaporation method. They claimed that the Seebeck coefficient, electrical conductivity and power factor were related to the substrate temperature. The maximum Seebeck coefficient at 25 °C (130 μV/K), electrical conductivity at 100 °C (650 $S{\cdot}cm^{-1}$) and the power factor at 150 °C (4 $\mu W/K^2{\cdot}cm$) have been obtained. The thermoelectric properties were attributed to the grain size variation versus the substrate temperature [30].

Li et al. [31] investigated the effect of SiGe alloy nanowires on the improvement of micro thermoelectric generators. They reported that the power factor of SiGe alloy nanowires is 10 $\mu W/K^2{\cdot}cm$ which is lower than the power factor of the $Bi_2Te_{2.7}Se_{0.3}$ compound (12 $\mu W/K^2{\cdot}cm$) produced in the current study. Meanwhile, Duan and Jiang [25] reported the maximum power factor of 12 $\mu W/K^2{\cdot}cm$ for

$Bi_2Te_{2.7}Se_{0.3}$ thin films produced by a flash evaporation method.

Ali et al. [32] fabricated ZnCuO nanostructure by hydrothermal method with a variation of Cu content. According to their research, the maximum power factor of 0.8 μW/K^2.cm was obtained for the compound with the highest concentration of Cu at 373 K. This value is lower than the power factor of $Bi_2Te_{2.7}Se_{0.3}$ thin films produced by Wudil et al. [24] using a pulsed laser deposition method (27 μW/K^2·cm) at 373 K. Seebeck coefficient of the thin films was reported about − 275 μV/K. Meanwhile, Kristiantoro et al. [33] fabricated Dy (dysprosium-rare earth element) -doped Bi_2Te_3 pellets by hydrothermal and sintering methods. A Seebeck coefficient of about -200 μV/K at 400 K was reported for the material.

Symeou et al. [34] manufactured Bi-doped Mg_2(-Si,Sn,Ge) bulk materials using ball milling and hot pressing methods. A power factor of 16 μW/K^2.cm has been obtained at 300 K. The power factor is higher than the power factor obtained by Duan and Jiang [25] for $Bi_2Te_{2.7}Se_{0.3}$ thin films (12 μW/K^2·cm).”

As mentioned above, in the field of thermoelectric materials, there are many studies conducted on the deposition of $Bi_2Te_{2.7}Se_{0.3}$ powder synthesized by hydrothermal and casting processes [14, 35, 36]. The results of the studies show that the powder characteristics play an important role in the thermoelectric properties of the manufactured thin films [14, 35]. In addition, some researchers have synthesized $Bi_2Te_{2.7}Se_{0.3}$ powder by milling process [18, 37]. There are enormous advantages in the production of $Bi_2Te_{2.7}Se_{0.3}$ milled powders from the aspects of purity, particle size distribution and grain size which influence on the thermoelectric properties of fabricated thin films. Although, production of thin films using milled powders has not been investigated. Therefore, it is worth fabricating $Bi_2Te_{2.7}Se_{0.3}$ thin film from milled powder in order to improve thermoelectric properties of this group of materials. The main object of the present study is the design of the procedure parameters for achieving a favorable power factor. Therefore, the deposition of $Bi_2Te_{2.7}Se_{0.3}$ powder synthesized by milling on a glass substrate using thermal evaporation procedure is one of the objects of the present research. Besides, investigation of the effect of the substrate temperature, before thermal evaporation deposition of the milled $Bi_2Te_{2.7}Se_{0.3}$ powder, and annealing of the produced thin films on thermoelectric properties of the films is other purpose of the current study. In conclusion, in the present research, thermoelectric properties of $Bi_2Te_{2.7}Se_{0.3}$ thin film materials produced from ball milled powder and deposited by different thermal evaporation parameters are investigated. In this regard, three subjects of milling of $Bi_2Te_{2.7}Se_{0.3}$ powder, thermal evaporation deposition of the milled powder and heat treatment of substrates and thin films are considered to reach the favorable thermoelectric properties. This research also aims to develop a foundation for the production of $Bi_2Te_{2.7}Se_{0.3}$ thermoelectric thin films with enhanced specifications.

2 Materials and methods

Bismuth (99.95%) powder, selenium (> 99.5%) powder as a dopant and tellurium (99.99%) powder used in this study were obtained from Sigma-Aldrich (Germany). The particle size distribution of the metallic powders was less than 150 μm. The $Bi_2Se_{0.3}Te_{2.7}$ powder was synthesized by mechanical alloying (MA) process. For synthesis of the nominal composition, pure Te, Bi and Se as raw materials were used according to the stoichiometry ratio of these elements. The powders were mixed in stainless-steel vials using a ball to powder ratio of 15:1 under an argon atmosphere with a speed of 300 rpm for 12 h in a planetary ball mill (PM 2400/Iran). The milling parameters have been selected based on the literature to reach the optimum thermoelectric properties [16, 18].

The synthesized powders were analyzed by X-ray diffraction (XRD) using AW_XDM300 diffractometer with Cu-Kα radiation (λ = 0.154 nm) and the data were collected in the 2θ range 20°–70°. Furthermore, the particle size of the milled powders was measured using particle size analyzer (Vasco3-Cordoun).

The deposition process of the ball milled powders was performed using a thermal evaporation instrument (EDS-160/Iran) by applying a current of 70 A to a tungsten boat and a deposition rate of 5 Å/s. In this study, the thermoelectric thin films with a thickness of 100 nm were prepared under chamber pressure of about 1×10^{-6} torr. The deposition parameters including the substrate temperature and the annealing temperature have been summarized in Table 1. It should be noted that the substrate temperature and annealing temperature have been selected based on the literature [23, 25, 29].

Microstructural study of the produced powders and thin films was carried out by a scanning electron microscopy (FESEM, TESCAN MIRA 30XMU) using an accelerating voltage of 10 kV using a secondary electron detector. The composition of the samples was investigated by energy dispersive X-ray spectra (EDS). Ultraviolet–visible (UV–Vis) spectra were obtained in the wavelength range 190–1100 nm by (Lambod UVD2950 UV spectrometer). Seebeck coefficient (S) of the samples was measured with the determination of temperature-voltage variation with a Seebeck instrument (SRM1)/Iran. Finally, the electrical conductivity (δ), carrier concentration and mobility were measured using the hall measurement system (Ecopia/Korea). The magnetic field was 0.5 Tesla with an input current of 2 mA, the temperature was selected in the range of room temperature to 480 K.

3 Results and discussion

3.1 Phase and structure

Figure 1 shows x-ray diffraction patterns of the mechanical alloyed $Bi_2Te_{2.7}Se_{0.3}$ powders and deposited thin films. Clearly, the main peaks of the $Bi_2Te_{2.7}Se_{0.3}$ milled powders are in agreement with the JCPDS code no.50.0954 [14]. It means that the x-ray diffraction patterns of powders show the $Bi_2Te_{2.7}Se_{0.3}$ compound formation without any impurity.

The patterns show that a rhombohedral crystal structure with: a = b = 4.47 Å, c = 30.424 Å has been formed during the milling, deposition procedure and after the annealing process [38, 39]. It can be seen that sample BS50W shows three peaks which are related to 23.08°, 27.75° and 37.39°, whereas the main peaks in sample BS50A50 corresponding to 27.90°, 38.24° and 43.67° (Fig. 1b). Figure 1b reveals three major peaks of 27.57°, 37.68° and 43.96° corresponding to the planes with an interplanar spacing of 3.23 Å, 2.38 Å and 2.05 Å, respectively, which is related to the thin film after the annealing process at the temperature 100 °C (sample BS100A100). As can be seen, the three main peaks of $Bi_2Te_{2.7}Se_{0.3}$ rhombohedral crystal structure of sample BS100W are located at 2Θ values of 23.15°, 27.90° and 37.65° corresponding to the planes with interplanar spacing of 3.83 Å, 3.20 Å and 2.39 Å, respectively. Furthermore, Fig. 1 clearly shows that the crystallinity of $Bi_2Te_{2.7}Se_{0.3}$ thin film improves after the annealing process. This fact can be observed with comparison of sample BS50A50 with BS50W and sample BS100A100 versus BS100W. Obviously, sample BS50W shows less crystallinity. It means a higher temperature is required for the formation of crystalline thin films. The improvement of crystallinity of thin films after the annealing process has been reported by Fan et al. [40] who produced Sb_2Te_3 thin films by ion beam sputtering method. In addition, Bourgault et al. [28] reported the enhancement of the crystallinity of $Bi_2Te_{2.7}Se_{0.3}$ thin film produced by magnetron sputtering method. The reason can be related to the elimination of defects.

According to Fig. 1b, the peaks of Bi_2Te_3 and Se are appeared in the unannealed samples. After the annealing process, the diffusion of Se atoms in Bi_2Te_3 occurs. Therefore, these peaks have been deleted in BS50WA50 and BS100A100 samples and the intensity of $Bi_2Te_{2.7}Se_{0.3}$ increases. However, in the BS50W sample due to the reduction of the substrate temperature, the Bi_2Te_3 peak is sensible at 23°.

The average grain size, or crystallite size, of thin films has been estimated using the Deby Scherrer formula, $D = {K\lambda}/{\beta Cos\theta}$ in which, K is a constant (0.89), λ is the wavelength of radiation = 1.54051 Å, β is the full width at half maximum and θ is the diffraction angle [36, 41]. Based on Table 2, the crystallite size after the annealing process (sample BS100A100: 92.9 Å) doesn't show more variation in comparison with the crystallite size before the annealing process (sample BS100W: 104.9 Å). Moreover, the number of crystallite per unit area (N) has been obtained based on the formula: $N = {d}/{D^3}$. In this

Table 1 The deposition parameters for $Bi_2Te_{2.7}Se_{0.3}$ thin film materials

Sample code ($Bi_2Te_{2.7}Se_{0.3}$ thin film)	Substrate temperature (°C)	Annealing temperature (°C)
BS50W	50	Without annealing
BS50A50	50	50
BS100W	100	Without annealing
BS100A100	100	100

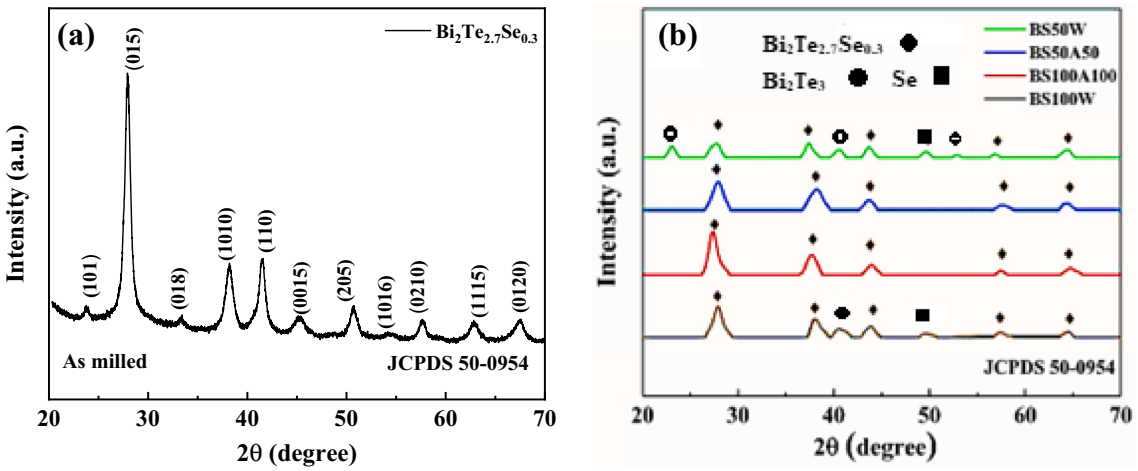

Fig. 1 XRD patterns of $Bi_2Se_{0.3}Te_{2.7}$ materials: **a** milled powders and **b** thin films

Table 2 The parameters obtained from x-ray analysis of $Bi_2Te_{2.7}Se_{0.3}$ thin film materials

Sample code ($Bi_2Te_{2.7}Se_{0.3}$thin film)	FWHM (°)	D (crystallite size) (Å)	Lattice strain (%)	*N* (Number of crystallites (cm^{-2})	δ (Dislocation density) (cm^{-2})
BS50W	0.7380	113.65	0.3	6.8×10^{11}	7.74×10^{11}
BS50A50	0.9840	83.19	0.4	1.7×10^{12}	1.44×10^{12}
BS100W	0.7872	104.9	0.33	8.7×10^{11}	9×10^{11}
BS100A100	0.8856	92.9	0.37	1.2×10^{12}	1.1×10^{12}

relationship, *D* is the grain size and d is the thin film thickness [22]. According to the equation, the number of crystallite per unit area ascends from 8.7×10^{11} cm^{-2} to 1.2×10^{12} cm^{-2} after the annealing process (sample BS100A100 in comparison with sample BS100W).

The lattice strain has been obtained by the formula: $\varepsilon = \beta Cos\theta/4$, in this relationship, ε is the lattice strain, β is the full width at half maximum and θ is the diffraction angle [22, 41]. The lattice strain before the annealing process (sample BS100A100) is 0.33% and after the annealing process (sample BS100W) is 0.37%. It means a slight variation in the lattice strain before and after the annealing process has been occurred. Furthermore, the amount of dislocation density (δ) can be obtained with: $\delta = {}^{1}/_{D^2}$ relationship, in which, D is the grain size [22]. As can be observed, the amount of dislocation density in sample BS100A100 compared with that of sample BS100W rises from 9×10^{11} cm^{-2} to 1.1×10^{12} cm^{-2} (Table 2). As a result, the maximum number of crystallites, dislocation density and lattice strain, and the minimum value of crystallite size is related to sample BS50A50. Moreover, grain refinement, elimination of large pores, formation of fine pores, and homogeneity of the microstructure occur in this sample.

3.2 Microstructural analysis

Figure 2 presents SEM images of $Bi_2Te_{2.7}Se_{0.3}$ powders synthesized by mechanical alloying procedure. The figure shows the flower like morphology of the spherical shape particles of $Bi_2Te_{2.7}Se_{0.3}$ with uniform particle size distribution. Besides, EDS results show that the Bi:Te:Se atomic ratio is 45:52:2.7. It can be seen that there is a little difference with the stoichiometric composition of $Bi_2Te_{2.7}Se_{0.3}$ compound which is 40:54:6. It means the chemical composition, especially the Bi content, shows a difference with a stoichiometric composition. Based on the study of Fu et al. [19], the flower like morphology of the powders similar to that obtained in this research, helps to the improvement of thermoelectric properties.

Figure 3 shows the particle size distribution of milled powders. The average particle size of the $Bi_2Te_{2.7}Se_{0.3}$ powder was obtained approximately 30.16 nm. Obviously, three mechanisms of cold

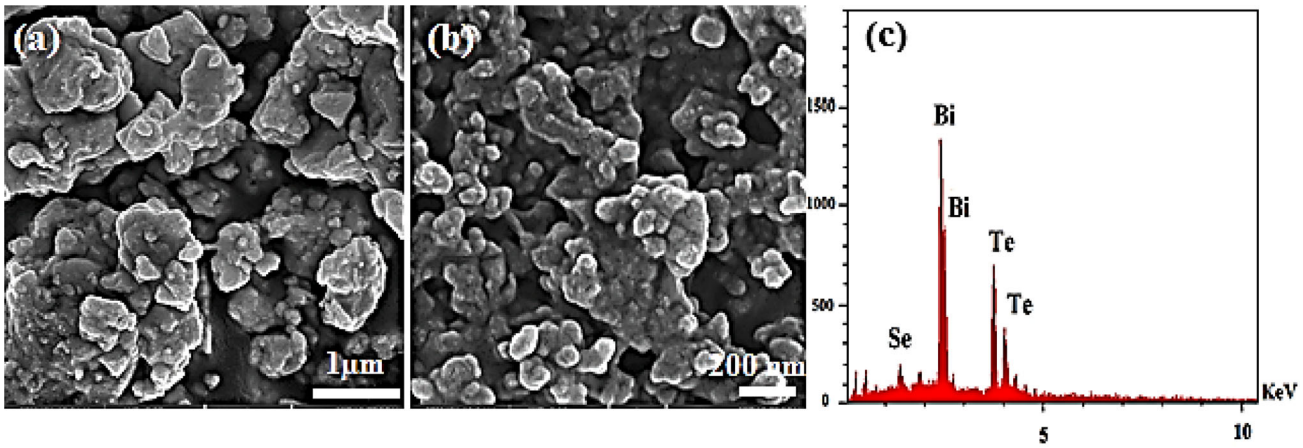

Fig. 2 **a**, **b** SEM micrographs of $Bi_2Se_{0.3}Te_{2.7}$ milled powder at different magnifications and **c** the relevant EDS spectra of the powder

deformation, welding and fracture occur during milling process. As a result, and according to Fig. 3, the produced milled powder shows a fine and uniform particle size distribution [11, 18, 39].

Figure 4 illustrates SEM images of $Bi_2Te_{2.7}Se_{0.3}$ thin films before and after annealing process. The sample BS50A50 microstructure shows a homogenous microstructure compared with that of sample BS50W. Furthermore, sample BS100A100 shows more homogeneity versus sample BS100W. Microstructural investigation of the thin film materials shows that the samples before and after annealing are well crystallized. However some large and small grains are observed in the thin films before the annealing process, the process helps to the homogeneity of the thin films. Therefore, it can be said that the annealing process leads to the elimination of defects and homogenization of the microstructure. It has been reported that the homogeneity of microstructure results in the improvement of thermoelectric properties of $Bi_2Te_{2.7}Se_{0.3}$ thin films [17].

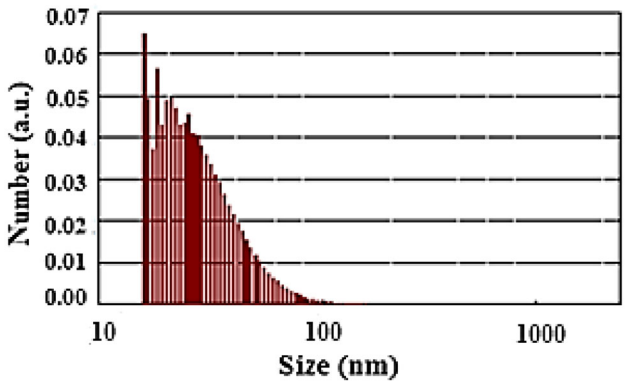

Fig. 3 Size distribution of $Bi_2Se_{0.3}Te_{2.7}$ milled powder

Comparison of BS50W and BS100W shows that the increase of the substrate temperature from 50 to 100 °C leads to the creation of some large precipitates of $Bi_2Te_{2.7}Se_{0.3}$ compound. In this regard, Wudil et al. [24] considered the effect of substrate temperature on the nucleation and growth rate of $Bi_2Te_{2.7}Se_{0.3}$ thin films. According to their report, an increase in the substrate temperature leads to the formation of large grains that grow at the expense of small ones. Based on the study, the larger pores are also formed with increasing the substrate temperature [24].

Figure 4 reveals that a dense structure consisting of nanograins is formed after the annealing process on the substrate (BS50A50). It can be seen that there are a lot of pores in the thin films before the annealing process. Duan et al. [25] reported that annealing process results in the grain growth and the elimination of pores. According to the author previous research [14], the pores presented in thin films lead to the decreasing of thermoelectric properties such as: Seebeck coefficient and electrical conductivity. Moreover, when sample BS100A100 is compared with BS100W, it is clear that the annealing process at 100 °C changes the nonhomogeneous microstructure to the microstructure with nanograins and some precipitates. According to EDS analysis (Table 3), the chemical composition of $Bi_2Te_{2.7}Se_{0.3}$ thin films before and after the annealing process is different. As can be seen, the Bi:Te:Se ratio in the $Bi_2Te_{2.7}Se_{0.3}$ thin films before the annealing process (sample BS50W) is 10:82:7, however after the annealing process (sample BS50A50) the ratio is 18:58.8:23. It means that the

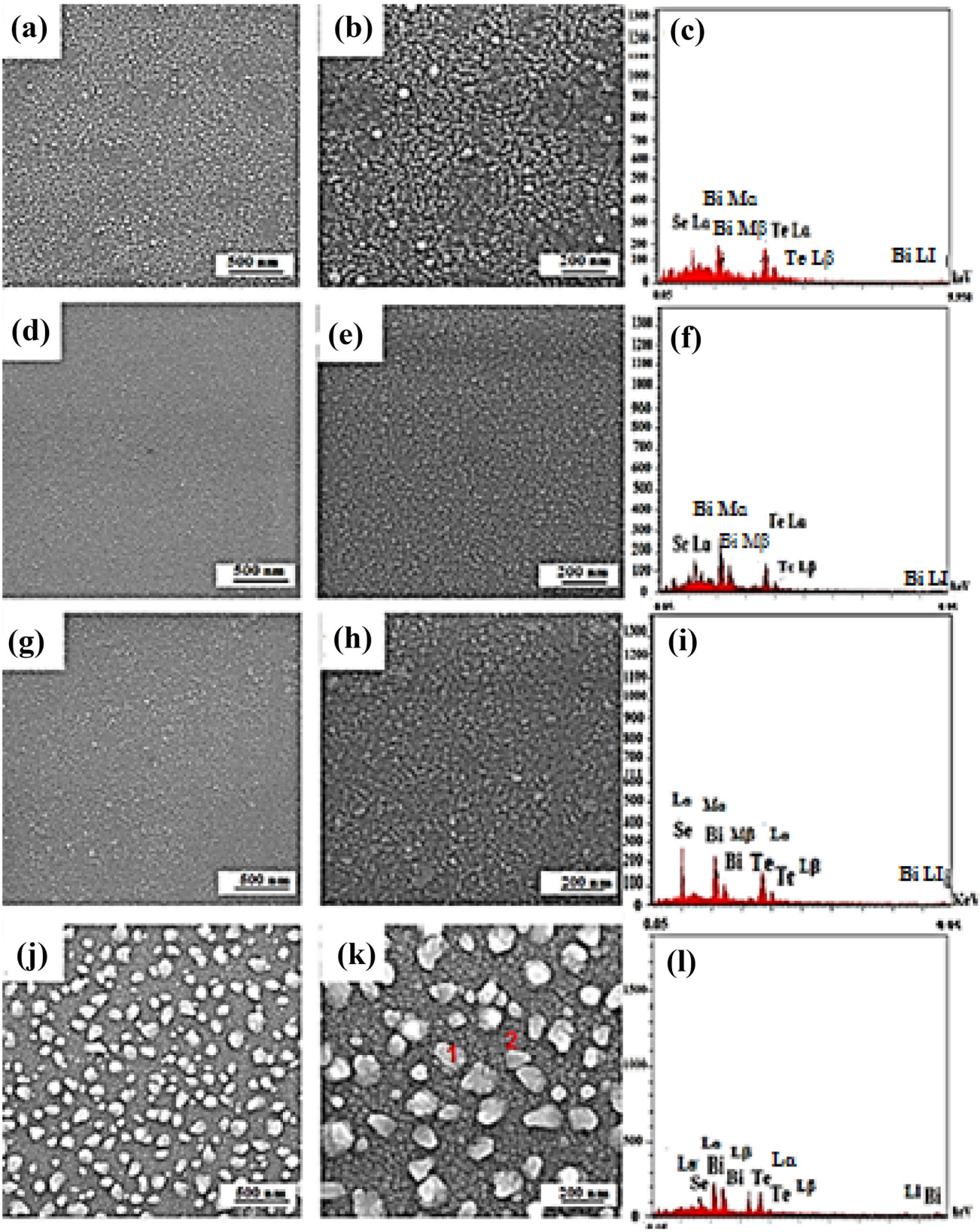

Fig. 4 SEM micrographs of $Bi_2Se_{0.3}Te_{2.7}$ thin film materials: **a**, **b**, **c** BS50W, **d**, **e**, **f** BS50A50, **g**, **h**, **i** BS100W and **j**, **k**, **l** BS100A100

Table 3 The relevant EDS spectra of thin film materials

Samples ($Bi_2Te_{2.7}Se_{0.3}$)	Bi (at. %)	Se (at. %)	Te (at. %)
Target	40	6	54
BS50W	7.45	10.43	82.12
BS50A50	23.21	17.94	58.85
BS100W	17.55	11.62	70.83
BS100A100 (precipitates)	32.65	10.63	56.72
BS100A100 (matrix)	37.5	5.7	56.81
powder	45	2.7	52

Bi:Te:Se ratio after the annealing process is closer to the stoichiometric composition of the compound. Therefore, it is clear that during annealing process, Se and Bi atoms diffuse and produce a composition with higher contents of Se and Bi and very close to the target composition.

The chemical composition of matrix and some precipitates in BS100A100 sample is shown in Table 3. It is clear that the matrix and precipitates show a chemical composition near to the chemical composition of target ($Bi_2Te_{2.7}Se_{0.3}$) however, because of the diffusion of Se and Bi atoms, the chemical composition of matrix is closer to the chemical composition of the target.

A similar result regarding the formation of Sb-rich phase during sputtering procedure of Sb_2Te_3 target on Si substrate has been reported by Fang et al. [23]. Based on the study, the crystalline precipitates with a higher content of Sb were detected. The size and amount of the Sb-rich precipitates were related to the annealing temperature performed on the thin films. In other words, a higher amount of the Sb-rich precipitates with the larger size came from the increase in the annealing temperature. They demonstrated that, applying the annealing process causes the more diffusion of Sb atoms and growth of the nuclei and also formation of nanoscale voids [23]. According to the literature, an increase in the annealing temperature results in the grain growth in Bi_2Te_3 based alloys [23, 25, 29].

Cross sections of $Bi_2Te_{2.7}Se_{0.3}$ thin films are shown in Fig. 5. As can be observed, the thickness of the films is around 100 nm for all the deposited thin films (before and after the annealing process). The main change is the formation of some precipitates during the annealing process.

Figure 6 displays EDS elemental maps of $Bi_2Te_{2.7}Se_{0.3}$ thin films. Obviously, three elements of tellurium, bismuth and selenium are distributed uniformly inside the thin films (before and after the annealing process). Besides, no any impurity has been detected. It means that the XRD and EDS results confirm the $Bi_2Te_{2.7}Se_{0.3}$ formation during milling and deposition processes.

Because, nanopores, homogeneity of grains and the near stoichiometric of thin films are the main factors affecting improvement of thermoelectric properties, it seems sample BS50A50 fabricated at the favorable substrate and annealing temperature can be selected as the best candidate from the chemical and microstructural aspects.

3.3 Optical properties

Figure 7 shows the results of ultraviolet–visible (UV–VIS) analysis of $Bi_2Te_{2.7}Se_{0.3}$ thin films. For calculation of the band gap energy, the Tauc's formula $\left(\propto hv = \left(hv - E_g\right)^n\right)$ was used. In this formula, C is a constant, h is the Planck constant, ν is the frequency and α is the absorption coefficient based on the UV–VIS intensity [5, 37, 42]. The exponent value (n) can be $\frac{1}{2}$, $\frac{3}{2}$, 2 or 3 for direct allowed, direct forbidden, indirect allowed or indirect forbidden transition, respectively. In this material, it was found that $n = \frac{1}{2}$ shows the best fitting (straight line) with Tauc's formula for $Bi_2Te_{2.7}Se_{0.3}$ thin film materials before and after the annealing process. Based on Tauc's equation, the values of the band gap for BS50W, BS50A50, BS100W and BS100W100 samples were obtained as: 0.99 eV, 0.82 eV, 0.89 eV and 0.88 eV, respectively. The results show that sample BS50W presents the highest band gap energy in comparison with the other samples. The main reason can be the non-homogenous structure of sample BS50W. Besides, the chemical composition of the sample is far from the stoichiometric composition. On the other hand, the band gap energy of the other thin films is almost the same. The band gap energies obtained in the present study for $Bi_2Te_{2.7}Se_{0.3}$ thin films are higher than the band gap calculated in the research carried out by Ali et al. [43] (0.15 eV). In that study, the production method was the physical vapor deposition of melted material. The nanograin structure of the thin films produced in the present study is the main reason for this difference. The effect of nanograin size on the increase of band gap energy is confirmed by comparing these results with the results of the thin films produced by other

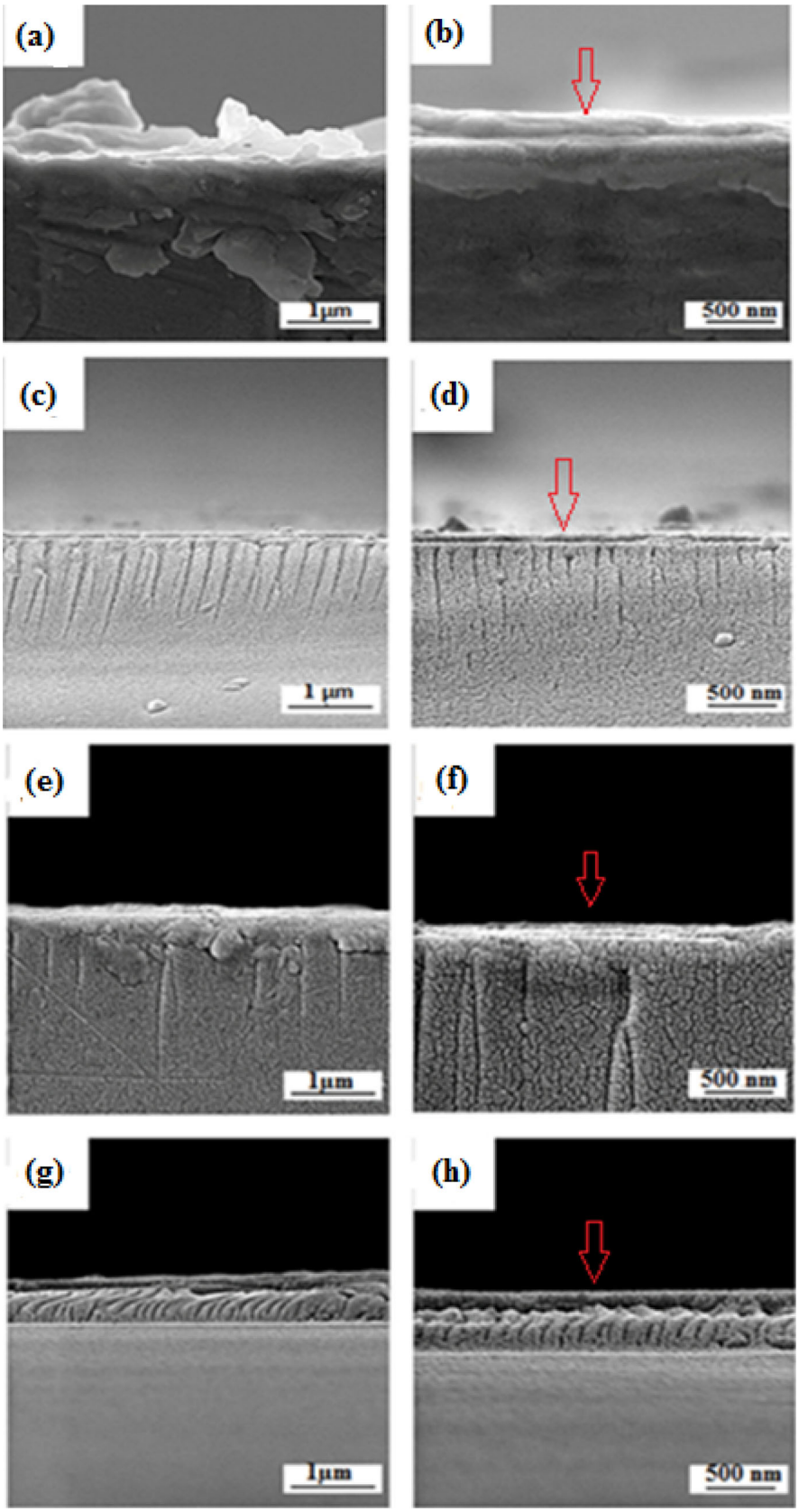

Fig. 5 Cross-sectional SEM images of thin film materials (illustrated by Red arrows): **a**, **b** sample BS50W, **c**, **d** sample BS50A50, **e**, **f** sample BS100W and **g**, **h** sample BS100A100 (Color figure online)

methods. For example, the $Bi_2Te_{2.7}Se_{0.3}$ thin films produced from the melted powders showed the lower band gap energy (0.52 eV) due to the larger particle size [5]. Therefore, the higher value of band gap obtained in the current study can be attributed to the finer grain size (nano) of the fabricated $Bi_2Te_{2.7}Se_{0.3}$ thin films.

3.4 Electrical transport properties

Electrical transport properties of the $Bi_2Te_{2.7}Se_{0.3}$ thin films are shown in Fig. 8. In this regard, the hall coefficient was obtained for the calculation of carrier concentration and mobility. Clearly, according to the literature [28, 40], the carrier concentration (p) and the Hall coefficient (R_H) are related by the equation $R_H = 1/pe$. In this relationship, e is the elementary charge. The mobility (μ) and the Hall coefficient are related by $\mu = R_H.\delta$ where, δ is the electrical conductivity. Figure 8a indicates the positive sign of the Hall measurement result. It means that holes play the carrier role in all of the samples.

Comparison of the carrier concentration of samples, before and after the annealing process, shows that the carrier concentration increases after the annealing process (sample BS50A50 versus BS50W and sample BS100A100 versus BS100W).

According to the literature [25, 44], Bi_2Te_3 crystal includes antistructure defects. Furthermore, based on Eq. (1), the interaction between vacancies and antisite defects plays the main role in the determination of the type of semiconductors (n type or p type):

$$2Bi_{Bi} + 3Te_{Te} \leftrightarrow 2Bi^{-}_{Te} + 3V^{+}_{Te} + 2V^{-1.5}_{Bi} + (3/2)Te_2 + 2h^{+}. \quad (1)$$

In this relationship, V and h are vacancy and hole concentration, respectively. Bi_{Bi} shows the Bi atoms, Te_{Te} shows the Te atoms, $Bi^{-}{}_{Te}$ shows the Bi atoms that occupy the Te vacancies, $V^{+}{}_{Te}$ is the sign of Te vacancies and $V^{-}{}_{Bi}$ is the sign of Bi vacancies. The sign of Te_2 shows the evaporation of Te. The antisites of Bi_{Te} are formed in Te vacancies. Therefore, based on Eq. (1), the annealing process leads to the Te evaporation and influences the production of vacancies and antisites. Hence, the increase of the carrier concentration in the present study shows the increase of the antistructures (Bi_{Te} as hole producers) due to the effect of annealing temperature. It means the annealing process results in the improvement of the thermoelectric properties due to the increasing carrier concentration. The sheet concentration at 305 K (4.53×10^{15} cm^{-2}) shows a higher value versus the thin films produced by thermal evaporation method using hydrothermally synthesized powders without the annealing process (1.99×10^{15} cm^{-2}) [14]. This can be attributed to the annealing process carried out in the present study and its effect on the antistructure sites [7, 26]. It means that the interaction of Te vacancies and antisites is facilitated with employing annealing treatment after the deposition of thin films. Besides the bulk carrier concentration obtained in this study for sample BS100A100 at room temperature (4.5×10^{20} cm^{-3}) is less than the value reported by Kim et al. [26] at annealing temperature of 373 K (10×10^{20} cm^{-3}). It should be mentioned that Kim et al. [26] fabricated p-type $Bi_{0.5}Sb_{1.5}Te_3$ thin films by flash evaporation procedure.

The mobility of thin films before and after the annealing process is shown in Fig. 8d. Clearly, comparison of mobility of sample BS100A100 with that of sample BS100W shows that the non-homogeneity in chemical composition of BS100A100 and its structure can be the main reasons for the lower mobility of the thin film after the annealing process at temperature 100 °C. The mobility of BS100A100 thin film in the present study at 305 K shows a lower value (4.89 $cm^2/(V{\cdot}s)$ compared with that of the thin film produced by other methods (8 $cm^2/(V{\cdot}s)$ as deposited thin film and 20 $cm^2/(V{\cdot}s)$ after annealing process at 323 K) [28]. The nano-size grains in the present study can be the factor for the lower mobility [28]. On the other hand, the scattering from grain boundaries is the main reason for the reduction of mobility. Notably, the high mobility (39.9 $cm^2/(V{\cdot}s)$) at room temperature can be observed in the sample BS50A50 compared with other samples. As mentioned before, the structural and chemical homogeneity, nanopores and slow grain growth are the factors for the higher mobility of sample BS50A50 at all the temperatures. The mobility of BS50A50 at room temperature is higher than the value reported in literature (20 $cm^2/(V{\cdot}s)$) [28]. It is worth noting that the fluctuations observed in the graphs of Fig. 8 are due to the effect of temperature resulting in the various interactions of antistructures and vacancies.

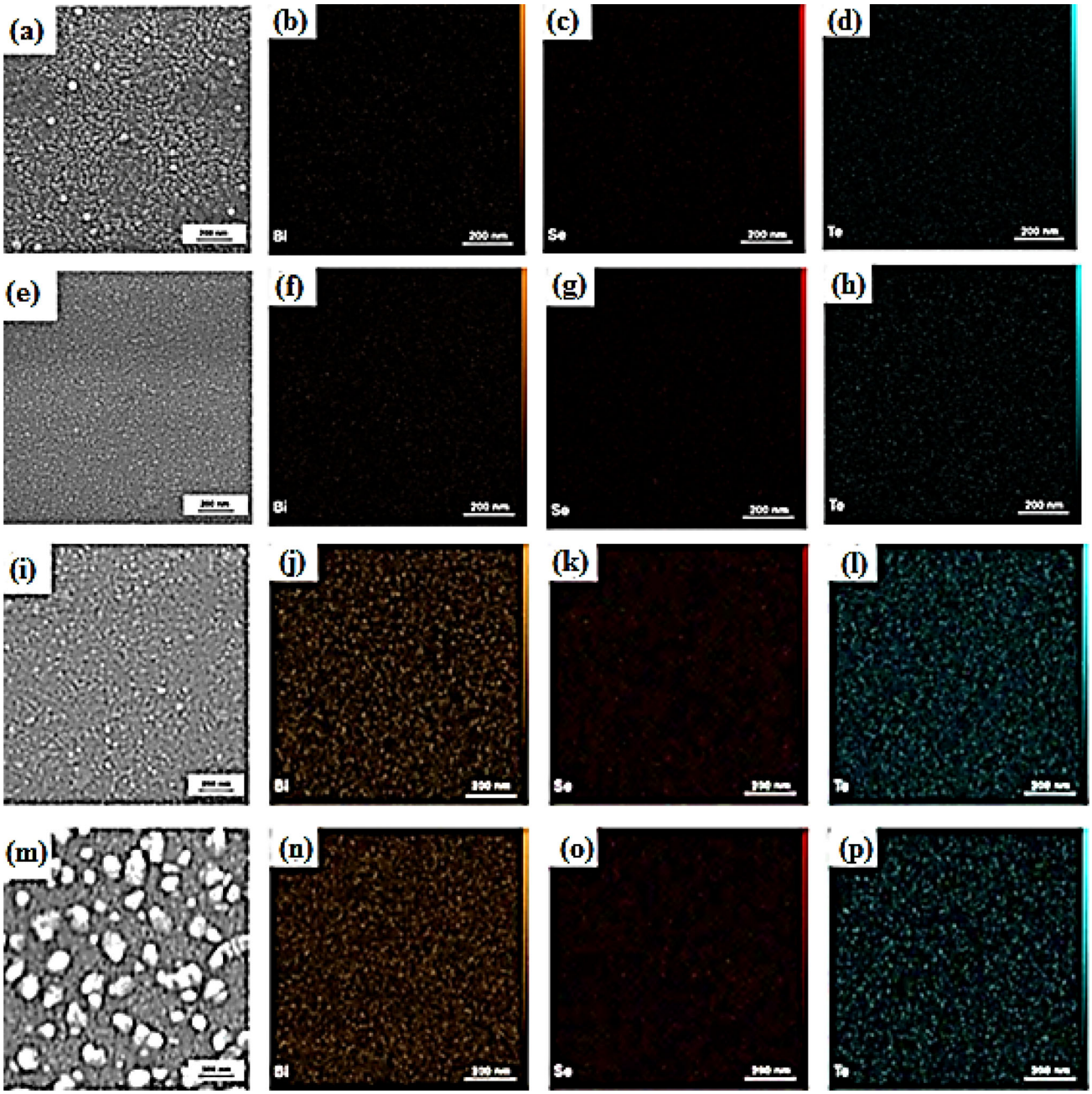

Fig. 6 FESEM image and EDS analysis of $Bi_2Se_{0.3}Te_{2.7}$ thin film materials: **a**, **b**, **c**, **d** sample BS50W, **e**, **f**, **g**, **h** sample BS50A50, **i**, **j**, **k**, **l** sample BS100W and **m**, **n**, **o**, **p** sample BS100A100

3.5 Electrical conductivity

Figure 9 shows the electrical conductivity and resistivity of the fabricated thin films. The electrical conductivity is obtained by the $\delta = ne\mu$ formula in which, n is the carrier concentration and μ is the mobility [38, 40]. It means that the increase in the carrier concentration leads to rising the electrical conductivity. Therefore, the higher electrical conductivity at room temperature (273 $(\Omega{\cdot}cm)^{-1}$) after annealing process at 100 °C (sample BS100A100) versus 106 $(\Omega{\cdot}cm)^{-1}$ for sample BS100W comes from the fact that the thin film has achieved a higher carrier concentration after annealing process. The higher electrical conductivity and lower resistivity of $Bi_2Te_{2.7}Se_{0.3}$ thin films are the positive aspects of annealing process. The higher electrical conductivity at room temperature are related to samples BS100A100 (273 $(\Omega{\cdot}cm)^{-1}$)

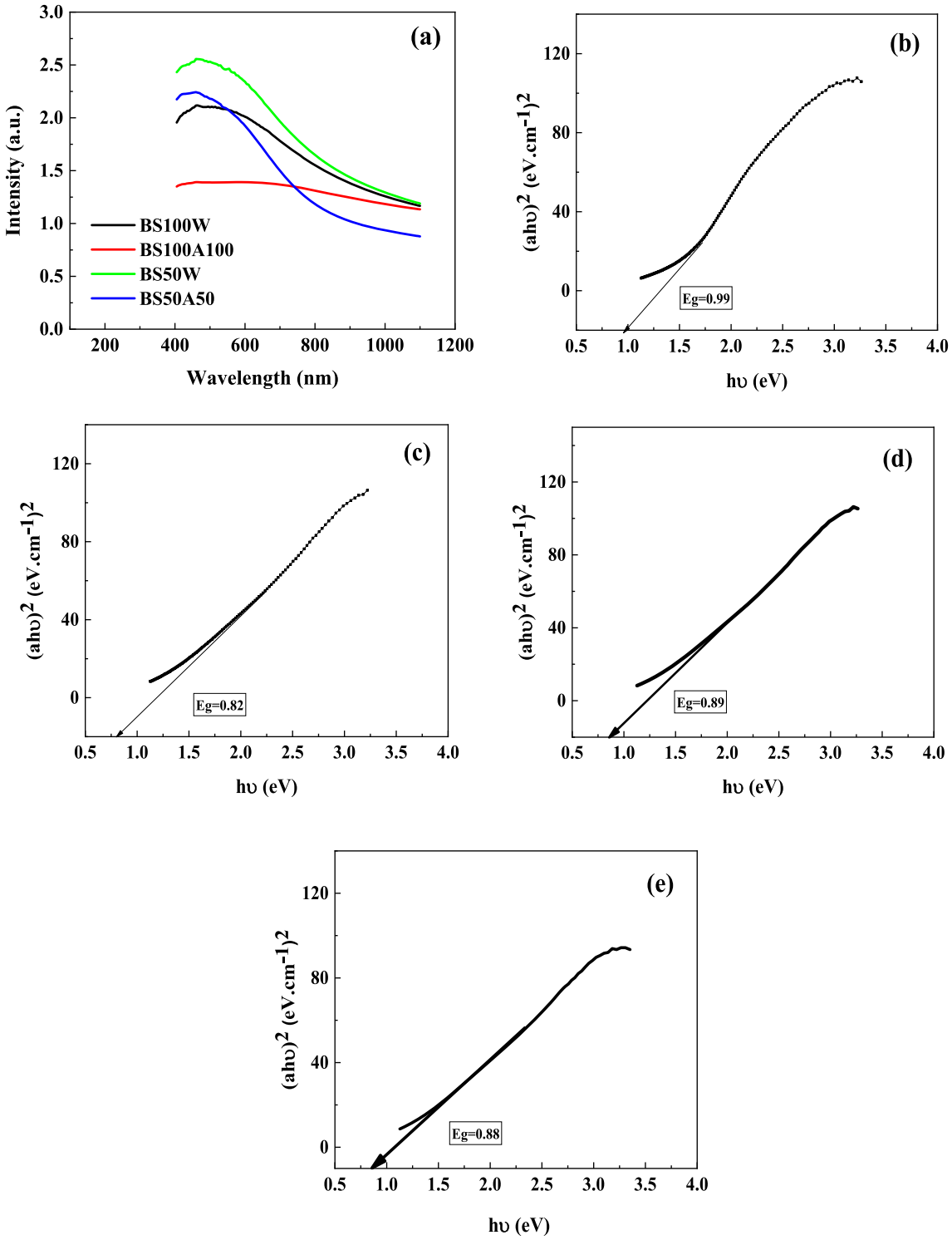

Fig. 7 **a** UV spectra of $Bi_2Se_{0.3}Te_{2.7}$ thin film materials, (b-e) plots of $(\alpha h\nu)^2$ as a function of hν for thin film materials: **b** BS50W, **c** BS50A50, **d** BS100W and **e** BS100A100

and BS50A50 (257 $(\Omega \cdot cm)^{-1}$). Besides, the value of the electrical conductivity in this research at room temperature is lower than the values of $Bi_2Te_{2.7}Se_{0.3}$ thin films reported in other studies [24, 25]. This can be attributed to the lower value of the mobility obtained in the present research due to the nanostructure of

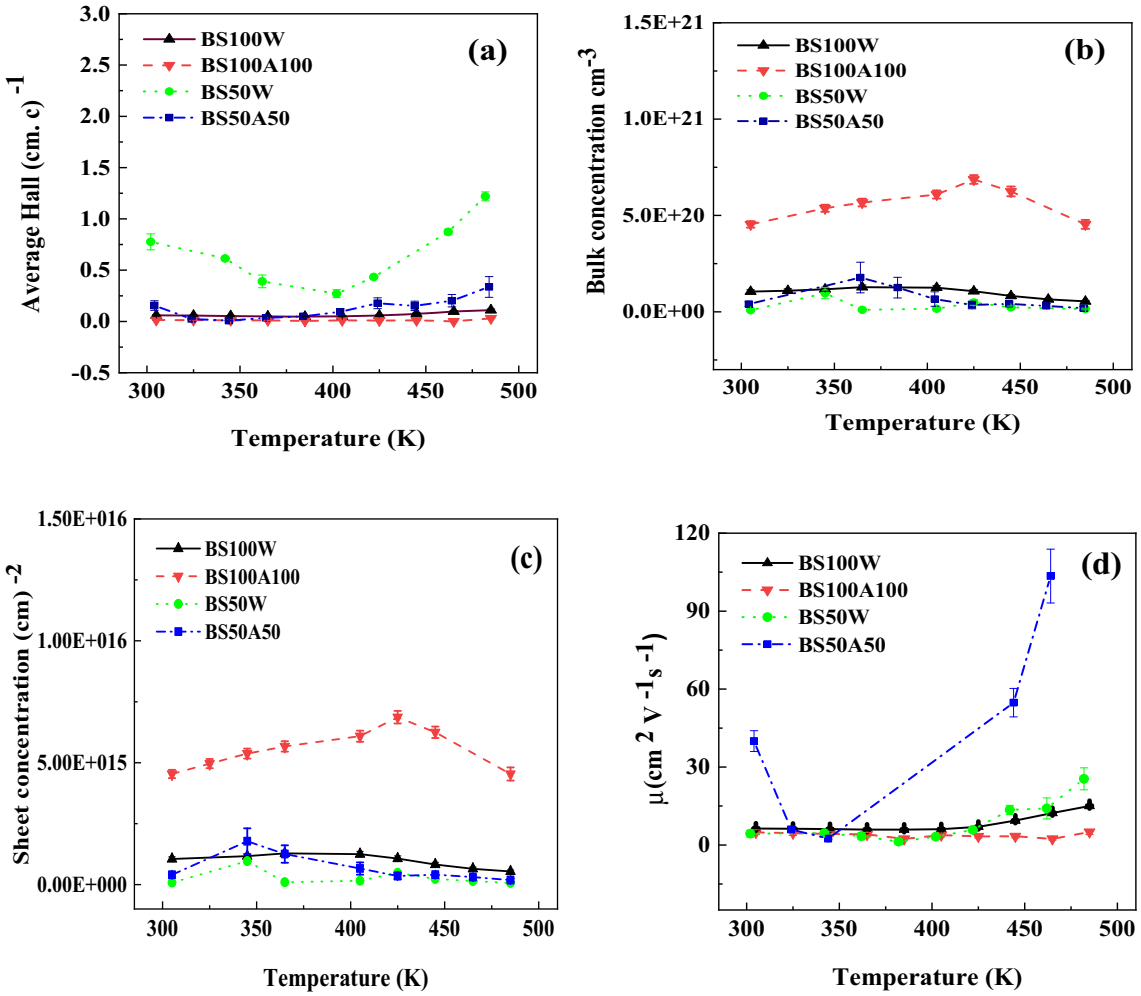

Fig. 8 The temperature dependence of: **a** average Hall coefficient, **b** bulk carrier concentration, **c** sheet concentration and **d** Mobility

the thin films. In other words, the high grain boundary area per unit volume of the fabricated thin films causes the low mobility values gained in the present research [24, 25]. In addition to these results, Han et al. [45] demonstrated that the nano grain size of thin films results in lower electrical conductivity compared to bulk materials with a larger grain size.

The trend of the electrical conductivity of the samples is related to the variation of the two factors of carrier concentration and mobility. For example, the reduction of the electrical conductivity of sample BS100A100 comes from the reduction of the mobility despite the increase of the carrier concentration. Similarly, the slight increase in the electrical conductivity of sample BS100W in the temperature range 300–470 K is due to the increase in the mobility despite the small drop of the carrier concentration. Besides, in the case of BS50A50, the reduction of the electrical conductivity at temperatures lower than 400 K can be related to the reduction of the mobility especially in the range 300–350 K and to the decrease of the carrier concentration especially in the range 350–400 K.

3.6 Seebeck coefficient

The Seebeck coefficient of thin film materials has been shown in Fig. 10. The positive sign of the Seebeck coefficient shows that the thin films are p-type semiconductor. The maximum Seebeck coefficient at room temperature belongs to sample BS50W with a value of 228 μV/K. The Seebeck coefficient of 59, 65 and 6.5 μV/K at 323 K have been obtained for samples BS50A50, BS100W and BS100A100, respectively. According to the author previous work, the Bi_{Te} antisites in the microstructure of thin films are the

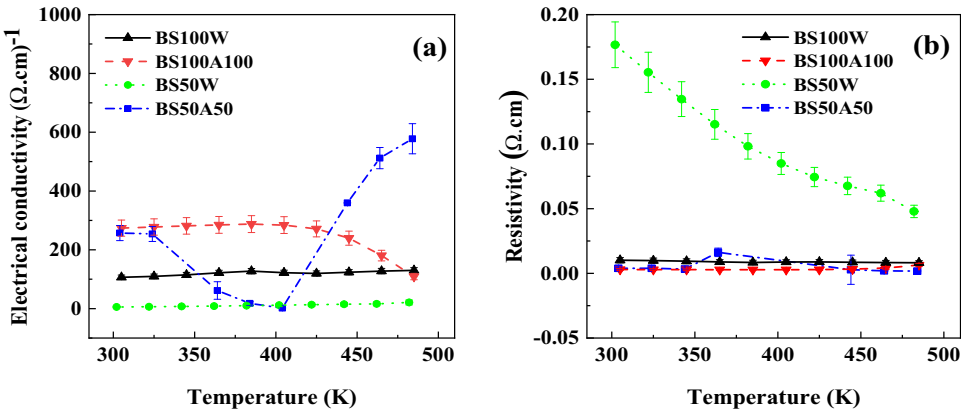

Fig. 9 Thermoelectric properties of fabricated thin films: **a** electrical conductivity and **b** resistivity

main factors for the positive sign of the Seebeck coefficient [14]. As can be found from formula 1, Bi_{Te} antisites as acceptors (hole producers) in the crystal structure and Te vacancies as donors (electron producers) can be balanced with the employ of annealing treatment on the substrate and deposition parameters. This can be clarified with the following formula in a thin film [37]:

$$2V''_{Bi} + 3V^{\circ\circ}_{Bi} + Bi'_{Te\leftrightarrow}Bi^{x}_{Bi} + V'''_{Bi} + 4V^{\circ\circ}_{Te} + 6e', \quad (2)$$

where, V and e are vacancy and electron concentration. On the other hand, V_{Bi} shows the Bi vacancies, V_{Te} shows the Te vacancies and Bi_{Te} shows the Bi atoms which occupy Te vacancies. Bi_{Bi} is the sign of Bi atoms. Hence, the hole concentration varies according to the interaction and balance of two factors of vacancies (V_{Te}) and antisites (Bi_{Te}, Se_{Te}). Based on Fig. 8, the maximum sheet concentration (4.5×10^{15} cm^{-2}) and the minimum Seebeck coefficient (6.5 μV/K) are related to sample BS100A100 at room temperature. Furthermore, the minimum sheet concentration (8×10^{13} cm^2) and the maximum Seebeck coefficient (228 μV/K) are related to sample BS50W at room temperature. Obviously, the relationship of the Seebeck coefficient and the carrier concentration is based on the formula (3) [24].

$$S = \frac{\left(-\pi k_B^2 m*\right).T}{\left((3\pi^2)^{2/3}\right).e.h^2.n^{2/3}}, \quad (3)$$

in which, k_B is the Boltzmann's constant, m ∗ is the effective mass, T is the temperature, h is the Plank constant and n is the carrier concentration. Therefore, the higher Seebeck coefficient comes from the lower carrier concentration.

Furthermore, according to the following equation the Seebeck coefficient is related to the Fermi level,

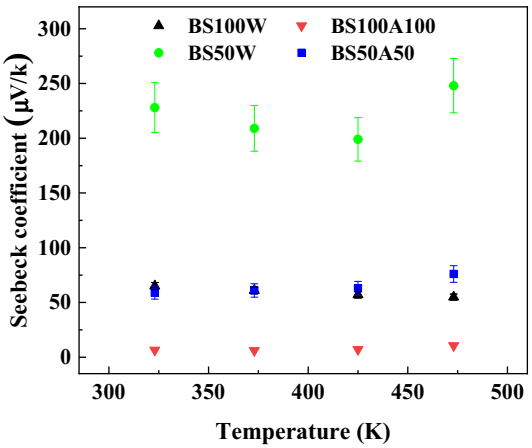

Fig. 10 Temperature dependence of Seebeck coefficients of $Bi_2Se_{0.3}Te_{2.7}$ thin film materials

scattering term and the carrier concentration. Therefore, the variation of the Seebeck coefficient is due to the variations of these three factors during the temperature change.

$$a = \pm k_B/e\left(5/2 + S - \eta*\right), \quad (4)$$

where, $\eta*$ is the reduced Fermi level and s is the scattering factor [46]. For example, the higher Seebeck coefficient up to 480 °C (10.6 μV/K) for sample BS100A100 after annealing at 100 °C is related to the low sheet concentration (4.5×10^{15} cm^{-2}) and the high mobility (103.5 cm^2/(V.s). The low positive Seebeck coefficient in BS100A100 (10.6 μV/K) is the sign of the Seebeck coefficient variation to the negative value at the higher annealing temperature. It can be predicted that the increase of the substrate temperature to higher than 100 °C and annealing of the thin films at more than 100 °C lead to the fabrication of n-type $Bi_2Te_{2.7}Se_{0.3}$ thin film conductors. The increasing trend of the Seebeck coefficient for

BS50A50 with increasing temperature is due to the increase of the mobility and decrease of the carrier concentration up to 480 °C. The low Seebeck coefficient (55 μV/K at 473 K) for sample BS100W can be attributed to the mechanism of the scattering of carriers. The scattering term determines the exponent of the energy dependence of the carrier mean free path. For the pure phonon or lattice vibration scattering of the carriers, s = 0 which can be divided into two terms of acoustical and optical phonon scattering. For the scattering of impurities (even ionized donors and acceptors), $s = 2$ and for mixed phonon and impurity scattering, $s = 1$. Besides, the reduced Fermi level is related to temperature, based on $\eta* = {}^{\eta}/_{k_B T}$, formula [46]. Therefore, the variation of Seebeck coefficient with temperature is due to the balance of the scattering mechanism, carrier density and the reduced Fermi level. The positive sign of the Seebeck coefficient is related to the valence band and the negative sign is attributed to the conduction band. The mobility variation according to $\mu = T^{(-3/2)+s}$ formula determines the scattering factor in semiconductor thin film materials [47].

In many studies, the effect of annealing process on the variation of Seebeck coefficient of Bi_2Te_3 based materials has been confirmed [7, 25, 35]. Moreover, the effect of heat treatment on the substrate on the Seebeck coefficient in other studies has been reported [24, 30]. The reason for the variation of the Seebeck coefficient is related to the influence of the annealing process on antisites and vacancies interaction as hole or electron sink [48]. For example, Yonezawa et al. [49] evaluated the effect of annealing process on Bi_2Te_3 thin films deposited by sputtering method. According to the research, the effect of a annealing temperature on the improvement of crystallinity, low defects and less evaporation of Te atoms has been proved. Moreover, the carrier concentration of thin films is adjusted with the annealing temperature. Furthermore, in the study done by Kim et al. [27] it was proved that the annealing process on $Bi_2Te_3Se_{0.5}$ thin films deposited by pulse electrodeposition method solves two problems in thin films. The first one is the improvement of crystal quality and the second one is the control of point defects.

Duan et al. [25] produced $Bi_2Te_{2.7}Se_{0.3}$ thin films by flash evaporation method. Based on the research, the role of annealing temperature in the reduction of the antisites was confirmed. Moreover, the Seebeck coefficient of – 160 μV/K at the annealing temperature of 373 K has been reported [25]. The negative sign of the Seebeck coefficient and the high value of this parameter show the low electron concentration in the thin films. Kuo et al. [37] fabricated Bi_2Te_3 bulk materials with milling and spark plasma sintering procedures. In that study, the change of the Seebeck coefficient from a positive value to a negative value was related to the milling time. It was confirmed that the milling time is effective on the size, distribution and lattice defects of the milled powders [37]. Therefore, the interaction of antisites (Bi_{Te} as hole producers) with Te vacancies was influenced by milling time. In this research the Seebeck values of 166 μV/K at 300 K and -8.9 μV/K at 500 K have been reported for Bi_2Te_3 bulk materials prepared by sintering procedure at 573 K, without milling process. Song et al. [7] investigated the annealing procedure effect on Bi_2Te_3 based material ($Bi_{0.45}Sb_{1.55}Te_3$ thin film) prepared by co-sputtering method. They found that an increase in the annealing temperature (from room temperature to 200 °C) results in the increase of the Seebeck coefficient from 150 to 250 μV/K. Moreover, they proved that ascent of the annealing temperature from 200 to 400 °C leads to the descent of the Seebeck coefficient from 250 to 150 μV/K.

In conclusion, different factors such as Fermi level, microstructure (nano and micron), grain size and interfaces, impurities, carrier concentration, mobility and the scattering factor affect Seebeck coefficient of the thermoelectric materials [48]. Some of these factors are changed by annealing temperature and thus, influence the Seebeck coefficient of thermoelectric materials.

3.7 Power factor

Figure 11 presents the power factor of $Bi_2Te_{2.7}Se_{0.3}$ thin films before and after annealing process. Clearly, the power factor of thin films can be calculated by the equation: $PF = \delta\alpha^2$ in which, δ is the electrical conductivity and α is the Seebeck coefficient [50, 51]. It can be seen that sample BS50A50 shows the highest power factor at room temperature (0.88 $\mu W/K^2 \cdot cm$). However, the lower power factor values of 0.33, 0.46, and 0.01 $\mu W/K^2 \cdot cm$ were obtained for samples BS50W, BS100W and BS100A100, respectively. The main reason for the higher power factor of BS50A50 is attributed to the high electrical conductivity (257 S/cm) and the favorable Seebeck coefficient (59 μV/

K). Comparison of the samples illustrates that samples BS50A50 and BS100W show two favorable thermoelectric characteristics such as electrical conductivity and Seebeck coefficient. Furthermore, the samples BS50W and BS100A100 don't show a balance between electrical conductivity and Seebeck coefficient. For example, sample BS50W shows the maximum Seebeck coefficient (228 μV/K) and the minimum electrical conductivity (5.7 (S/cm)). On the contrary, BS100A100 showed the minimum Seebeck coefficient (6.5 μV/K) and the maximum electrical (273 (S/cm)) conductivity. The homogeneity of microstructure, crystallinity and suitable grain size are the reasons for the highest power factor of sample BS50A50.

Lin et al. [50] fabricated Sb_2Te_3 thin films by thermal evaporation method at a current of 50 A as a p-type conductor. According to the research, a Seebeck coefficient 28 μV/K and a power factor of 0.46 $\mu W/K^2.cm$ were obtained at room temperature. It is obvious that the higher thermoelectric power factor of $Bi_2Te_{2.7}Se_{0.3}$ thin films produced in the present study is due to its higher Seebeck coefficient (59 μV/K).

Mansouri et al. [17] fabricated $Bi_{0.5}Sb_{1.5}Te_3$ bulk material by spark plasma sintering method of the powders synthesized by mechanical milling. They reached a power factor of less than 0.4 $\mu W/K^2.cm$ for a p-type conductor. The lower power factor can be attributed to the lower electrical conductivity (4.48 S/cm) in comparison with those obtained in the present research.

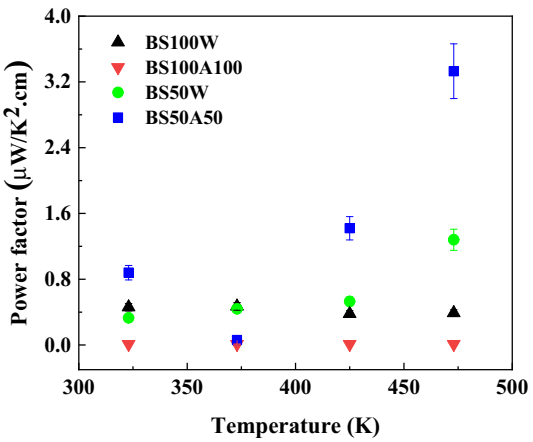

Fig. 11 Temperature dependence of power factor of $Bi_2Se_{0.3}Te_{2.7}$ thin film materials

Based on the results of the Seebeck coefficient (6.5 μV/K) and power factor (0.01 $\mu W/K^2.cm$) for sample BS100A100, it is anticipated that the higher temperature leads to the variation of p-conductor to n-conductor in the fabricated thin films. Therefore, it is possible to change the type of $Bi_2Te_{2.7}Se_{0.3}$ thin films from p-type to n-type with an annealing treatment. In this regard, Kuo et al. [37] proved the transition of the semiconductor in their research. They confirmed the effect of the production method on the transition of p-type conductor to n-type conductor in Bi_2Te_3 bulk materials. The production method included ball milling and spark plasma sintering (SPS) methods. In that research, the effect of the milling time on antisites and vacancies as well as the carrier concentration has been reported [37].

The maximum power factor (0.88 $\mu W/K^2.cm$) obtained in the present study, is higher than the power factor value reported by Bourgault et al. [51] (0.52 $\mu W/K^2.cm$). In that study, $Bi_2Te_{2.7}Se_{0.3}$ thin films were deposited on glass substrate by magnetron sputtering method. The thickness of the thin film, the time of sputtering and the plasma power have been selected as: 1100 nm, 60 min and 15 W, respectively. Furthermore, Lin et al. [50] produced Sb_2Te_3 thin films by thermal evaporation method and obtained a power factor of 0.5 $\mu W/K^2.cm$ [50]. It has been reported that $Bi_{0.2}Sb_{1.8}Te_3$, $Bi_{0.3}Sb_{1.7}Te_3$ and $Bi_{0.5}Sb_{1.5}Te_3$ bulk thermoelectric materials fabricated by milling and spark plasma sintering procedure show power factors of 0.06, 0.01 and 0.29 $\mu W/K^2.cm$, respectively [17]. The higher power factor reported in the current study can be attributed to the high Seebeck coefficient and the favorable electrical conductivity due to the annealing process after the deposition process and the substrate heat treatment.

In conclusion, the role of different factors including grain size, balance of the antisities and Te vacancies, crystallinity and near-stoichiometric composition has been verified in improvement of power factor of thin films. These parameters are mainly affected by annealing parameters such as temperature and time (see Table 4).

3.8 Electronic thermal conductivity

The values of electronic thermal conductivity of $Bi_2Te_{2.7}Se_{0.3}$ thin films have been presented in Fig. 12. Clearly, the total thermal conductivity (K_t) can be calculated by the equation of: $K_t = K_e + K_l$, in which,

Table 4 Thermoelectric properties of $Bi_2Te_{2.7}Se_{0.3}$ thin film materials at room temperature

Sample code ($Bi_2Te_{2.7}Se_{0.3}$ thin film)	Substrate temperature (°C)	Annealing temperature (°C)	S (μV/K)	Σ $(\Omega.cm)^{-1}$	PF μW/K^2·cm
BS50W	50	Without annealing	228	6.4	0.30
BS50A50	50	50	59	254	0.88
BS100W	100	Without annealing	65	110	0.46
BS100A100	100	100	6.5	277.6	0.01

K_l is the lattice thermal conductivity and K_e is the electronic thermal conductivity [52, 53]. The electronic thermal conductivity can be obtained from the equation: $K_e = LT\delta$ in which, L is the Lorentz factor equal to 2.44×10^{-8} WΩ/K^2. δ is the electrical conductivity and T is the temperature [52, 53]. Although, based on a report presented by Kim et al. [53], the relationship between the Lorentz number and the Seebeck coefficient according to the SPB model can be obtained by $L = \left(1.5 + \exp\left(-|S|/116\right)\right) \times 10^{-8}$ formula. Using the above formula, the Lorentz number is obtained as: 1.64×10^{-8}, 2.10×10^{-8}, 2.07×10^{-8} and 2.44×10^{-8} WΩ/K^2 at room temperature for samples BS50W, BS50A50, BS100W and BS100A100, respectively. In the presented research, among the calculated values, the higher value of Lorentz factor (2.44×10^{-8} WΩ/K^2) was considered in the determination of the electronic thermal conductivity.

It is clear that the electronic thermal conductivity of $Bi_2Te_{2.7}Se_{0.3}$ thin films before the annealing process is lower compared to that parameter for the annealed ones. Electrical conductivity improves by annealing process and this is the main reason for the higher thermal conductivity obtained after the annealing process. The comparison of the electronic thermal conductivity of thin films (0.001–0.002 W/cm·K) at room temperature shows that the parameter values are lower compared to the reported values for bulk materials (0.008, 0.005 and 0.004 W/cm·K) [15, 38, 54]. However, some studies reported the lower values of electronic thermal conductivity (3×10^{-7} and 1.5×10^{-4} W/cm·K) at room temperature [12, 14].

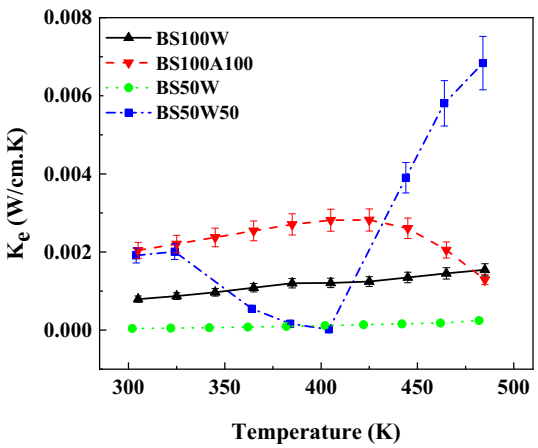

Fig. 12 Temperature dependence of the electronic thermal conductivity of $Bi_2Se_{0.3}Te_{2.7}$ thin film materials

4 Conclusions

In this study, the effect of the deposition parameters including substrate temperature and annealing temperature on the thermoelectric properties of $Bi_2Te_{2.7}Se_{0.3}$ thin films produced by thermal evaporation method of milled powders was investigated. The results have been summarized as follows:

1. The crystallinity and homogeneity of thin films improved after the annealing process.
2. The highest value of Seebeck coefficient (228 μV/K) was obtained for sample BS50W. Moreover, samples BS50A50 and BS100W showed the favorable Seebeck coefficients of 59 μV/K and 65 μV/K, respectively.
3. The highest electrical conductivity was related to sample BS100A100 due to the improvement of the crystallinity. The electrical conductivity of sample BS50A50 was closest to that of BS100A100. Therefore, the effect of the annealing process was sensible.
4. The enhanced power factor of BS50A50 (0.88 μW/K^2·cm) was due to the appropriate thermoelectric and microstructural properties.
5. The results of the present research led to the growth of the science for the improvement of the efficiency of thermoelectric devices.

Acknowledgements

The authors appreciate the support from Ferdowsi University of Mashhad (FUM).

Author contributions

All authors contributed to the study conception and design. Material preparation, data collection and analysis were performed by YS, and SAS. The first draft of the manuscript was written by YS, and SAS commented on previous versions of the manuscript. All authors read and approved the final manuscript.

Funding

The authors declare that no funds, grants, or other support were received during the preparation of this manuscript.

Data availability

Data sharing not applicable to this article as no datasets were generated or analysed during the current study.

Declarations

Conflict of interest The authors have no relevant financial or non-financial interests to disclose.

References

1. Ch. Zhang, F. Wei, X. Zhang, W. Chen, Ch. Chen, J. Hao, B. Jia, J. Solid State Chem. (2022). https://doi.org/10.1016/j.jssc.2022.123447
2. A. Azouaoui, A. Hourmatallah, N. Benzakour, K. Bouslykhane, J. Solid State Chem. (2022). https://doi.org/10.1016/j.jssc.2022.123020
3. J. Zheng, S. Chen, K. Cai, J. Yin, S. Shen, Ceram. Int. (2017). https://doi.org/10.1016/j.ceramint.2017.01.085
4. Y. Dingfeng, T. Yurou, Y. Hengquan, L. Wensheng, Z. Bin, Y. Wei, W. Guoyu, Z. Xiaoyuan, J. Solid State Chem. (2022). https://doi.org/10.1016/j.jssc.2022.123342
5. H. Mamur, M. Bhuiyan, Int. sci. Vocat. Stud. J. (2019)
6. X. Liu, W. Zhao, H.-Y. Zhou, S. Mu, D.-Q. He, W.-T. Zhu, P. Wei, H. Wu, Q.-J. Zhang, J. Electron. Mater. (2016). https://doi.org/10.1007/s11664-015-4027-7
7. J. Song, X. Chen, Y. Tang, Q. Yao, L. Chen, J. Electron. Mater. (2012). https://doi.org/10.1007/s11664-012-2228-x
8. Z.-H. Zheng, D. Yang, P.-C. Zhang, F. Li, Y.-X. Chen, G.-X. Liang, P. Fan, Mater. Lett. (2020). https://doi.org/10.1016/j.matlet.2020.128143
9. Q. Zou, H. Shang, D. Huang, T. Li, B. Xie, H. Gu, F. Ding, Soft. Sci. (2021). https://doi.org/10.20517/ss.2021.04
10. S. Masoumi, A. Noori, M. Shokrani, F. Hossein-Babaei, IEEE Trans. Instrum. Meas. (2020). https://doi.org/10.1109/TIM.2019.2931066
11. A. Soni, Z. Yanyuan, Y. Ligen, M.K.K. Aik, M.S. Dresselhaus, Q. Xiong, Nano Lett. (2012). https://doi.org/10.1021/nl2034859
12. A.M. Adam, E. Lilov, P. Petkov, Superlattices Microstruct. (2017). https://doi.org/10.1016/j.spmi.2016.09.034
13. Y. Saberi, S.A. Sajjadi, H. Mansouri, J. Mater. Sci. Mater. Electron. (2020). https://doi.org/10.1007/s10854-020-04435-y
14. Y. Saberi, S.A. Sajjadi, H. Mansouri, Ceram. Int. (2021). https://doi.org/10.1016/j.ceramint.2020.12.285
15. C. Kim, C.E. Kim, J.Y. Baek, D.H. Kim, J.T. Kim, J.H. Ahn, D.H. Lopez, T. Kim, H. Kim, Ind. Eng. Chem. Res. (2016). https://doi.org/10.1021/acs.iecr.6b00933
16. N. Bolghanabadi, S.A. Sajjadi, A. Babakhani, Y. Saberi, J. Electron. Mater. (2021). https://doi.org/10.1007/s11664-020-08656-z
17. H. Mansouri, S.A. Sajjadi, A. Babakhani, Y. Saberi, J. Mater. Sci.: Mater. Electron. (2021). https://doi.org/10.1007/s10854-021-05645-8
18. Y. Pan, J.F. Li, NPG Asia Mater. (2016). https://doi.org/10.1038/am.2016.67
19. J. Fu, S. Song, X. Zhang, F. Cao, L. Zhou, X. Li, H. Zhang, Cryst. Eng. Comm. (2012). https://doi.org/10.1039/c2ce06348d
20. H.S. Kim, S.J. Hong, J. Alloys Compd. (2014). https://doi.org/10.1016/j.jallcom.2013.05.163
21. K.C. Park, P. Dharmaiah, H.S. Kim, S.J. Hong, J. Alloys Compd. (2017). https://doi.org/10.1016/j.jallcom.2016.09.106
22. A.M. Adam, J. Alloys Compd. (2018). https://doi.org/10.1016/j.jallcom.2018.06.159
23. B. Fang, Z. Zeng, X. Yan, Z. Hu, J. Mater. Sci.: Mater. Electron. (2013). https://doi.org/10.1007/s10854-012-0888-1
24. Y.S. Wudil, M.A. Gondal, S.G. Rao, S. Kunwar, A.Q. Alsayoud, Ceram. Int. (2020). https://doi.org/10.1016/j.ceramint.2020.06.196

25. X. Duan, Y. Jiang, Appl. Surf. Sci. (2010). https://doi.org/10.1016/j.apsusc.2010.05.069
26. I.H. Kim, Mater. Lett. (2000). https://doi.org/10.1016/S0167-577X(00)00005-7
27. J. Kim, K.H. Lee, S.W. Kim, J.H. Lim, J. Alloys Compd. (2019). https://doi.org/10.1016/j.jallcom.2019.01.301
28. D. Bourgault, B. Schaechner, C. Giroud Garampon, T. Crozes, N. Caillault, L. Carbone, J. Alloys Compd. (2014). https://doi.org/10.1016/j.jallcom.2014.01.172
29. J.M. Lin, Y.C. Chen, C.P. Lin, J. Nanomater. (2013). https://doi.org/10.1155/2013/201017
30. J.M. Lin, Y.C. Chen, C.F. Yang, W. Chen, J. Nanomater. (2015). https://doi.org/10.1155/2015/135130
31. Y. Li, G. Wang, M. Akbari-Saatlu, M. Procek, H.H. Radamson, Front. Mater. (2021). https://doi.org/10.3389/fmats.2021.611078
32. H.T. Ali, M. Amami, U. Rehman, K. Mahmood, M. Yusuf, S. Ikram, A. Ali, N. Amin, K. Javaid, M. Imran Arshad, J. Phys. Chem. Solids (2022). https://doi.org/10.1016/j.jpcs.2021.110535
33. T. Kristiantoro dedi, V. Fauzia, J. Phys. Chem. Solids. (2021). https://doi.org/10.1016/j.jpcs.2021.110241
34. E. Symeou, M. Karyou, A. Delimitis, M. Constantinou, G. Constantinides, Ch. Nicolaou, I. Giapintzakis, Th. Kyratsi, J. Phys. Chem. Solids. (2022). https://doi.org/10.1016/j.jpcs.2021.110472
35. S. Kianwimol, R. Sakdanuphab, N. Chanlek, A. Harnwunggmoung, A. Sakulkalavek, Surf. Coat. Technol. (2020). https://doi.org/10.1016/j.surfcoat.2020.125808
36. A.M. Adam, P. Petkov, Ceram. Int. (2017). https://doi.org/10.1016/j.ceramint.2017.05.143
37. C.H. Kuo, C.S. Hwang, M.S. Jeng, W.S. Su, Y.W. Chou, J.R. Ku, J. Alloys Compd. (2010). https://doi.org/10.1016/j.jallcom.2010.02.171
38. D. Li, X.Y. Qin, Y.C. Dou, X.Y. Li, R.R. Sun, Q.Q. Wang, L.L. Li, H.X. Xin, N. Wang, N.N. Wang, C.J. Song, Y.F. Liu, J. Zhang, Scr. Mater. (2012). https://doi.org/10.1016/j.scriptamat.2012.04.005
39. A.Y. Eum, I.H. Kim, S.M. Choi, Y.S. Lim, W.-S. Seo, J.S. Park, S.H. Yang, J. Korean Phys. Soc. (2015). https://doi.org/10.3938/jkps.66.1726
40. P. Fan, Z.H. Zheng, G.X. Liang, D.P. Zhang, X.M. Cai, J. Alloys Compd. (2010). https://doi.org/10.1016/j.jallcom.2010.06.046
41. V.S. Vinila, R. Jacob, A. Mony, H.G. Nair, S. Issac, S. Rajan, A.S. Nair, J. Isac, Cryst. Struct. Theory Appl. (2014). https://doi.org/10.4236/csta.2014.31001
42. A. Azzouzi, M. Benchikhi, R. El Ouatib, Ceram. Int. (2020). https://doi.org/10.1016/j.ceramint.2020.06.144
43. H.M. Ali, E.M.M. Ibrahim, M.M. Wakkad, M.A.A. Mohamed, Optik (2018). https://doi.org/10.1016/j.ijleo.2017.12.090
44. S.-S. Lin, C.-N. Liao, J. Appl. Phys. (2011). https://doi.org/10.1063/1.3658256
45. S.T. Han, P. Rimal, C.H. Lee, H.-S. Kim, Y. Sohn, S.-J. Hong, Intermetallics (2016). https://doi.org/10.1016/j.intermet.2016.08.006
46. Y. Mishima, Y. Kimura, S.W. Kim, *Nanomaterials: from research to applications*, 1st edn. (Elsevier Science, Amsterdam, 2006), pp.383–389
47. K. Hasezaki, T. Hamachiyo, M. Ashida, T. Ueda, Y. Noda, Mater. Trans. (2010). https://doi.org/10.2320/matertrans.MH200901
48. H. Mansouri, Y. Saberi, S.A. Sajjadi, J. Electron. Mater. (2021). https://doi.org/10.1007/s11664-021-09332-6
49. S. Yonezawa, T. Tabuchi, M. Takashiri, J. Alloys Compd. (2020). https://doi.org/10.1016/j.jallcom.2020.155697
50. J.M. Lin, Y.C. Chen, W. Chen, J. Nanomater. (2015). https://doi.org/10.1155/2015/564954
51. D. Bourgault, C.G. Garampon, N. Caillault, L. Carbone, J.A. Aymami, Thin Solid Films (2008). https://doi.org/10.1016/j.tsf.2008.06.001
52. P. Dharmaiah, H.S. Kim, C.H. Lee, S.J. Hong, J. Alloys Compd. (2016). https://doi.org/10.1016/j.jallcom.2016.05.340
53. H.S. Kim, Z.M. Gibbs, Y. Tang, H. Wang, G.J. Snyder, APL Mater. (2015). https://doi.org/10.1063/1.4908244
54. E.B. Kim, P. Dharmaiah, K.H. Lee, C.H. Lee, J.H. Lee, J.K. Yang, D.H. Jang, D.S. Kim, S.J. Hong, J. Alloys Compd. (2019). https://doi.org/10.1016/j.jallcom.2018.10.408